INTERNATIONAL JOURNAL FOR NUMERICAL METHODS IN ENGINEERING, VOL. 34, 365–389 (1992)

ANALYSIS OF ORTHOGONAL METAL CUTTING PROCESSES

T. TYAN* AND WEI H. YANG†

Department of Mechanical Engineering and Applied Mechanics, The University of Michigan, Ann Arbor, Michigan 48109, U.S.A.

SUMMARY

The orthogonal metal cutting process for a controlled contact tool is simulated using a limit analysis theorem. The basic principles are stated in the form of a primal optimization problem with an objective function subjected to constraints of the equilibrium equation, its static boundary conditions and a constitutive inequality. An Eulerian reference co-ordinate is used to describe the steady state motion of the workpiece relative to the tool. Based on a duality theorem, a dual functional bounds the objective functional of the primal problem from above by a sharp inequality. The dual formulation seeks the least upper bound and thus recovers the maximum of the primal functional theoretically. A finite element approximation of the continuous variables in the dual problem reduces it to a convex programming. Since the original dual problem admits discontinuous solutions in the form of bounded variation functions, care must be taken in the finite element approximation to account for such a possibility. This is accomplished by a combined smoothing and successive approximation algorithm. Convergence is robust from any initial iterate. Results are obtained for a wide range of control parameters including cutting depth, rake angle, rake length and friction. The converged solutions provide information on cutting force, chip thickness, chip stream angle and shear angle which agree well both in values and trend with the published data. But the available data represent only a small subset in the range of parameters exhaustively investigated in this paper.

INTRODUCTION

Manufacturing technology has been a driving force behind modern economies since the Industrial Revolution (1770). Metal forming processes, in particular, have created machinery and structures that permeate almost every aspect of human life today. Although manufacturing techniques have become more sophisticated, many processes and tool designs are still based on experience and intuition. Advances in computer and material sciences have greatly enhanced our ability to develop predictive capability and to achieve the goal of optimization for a wide variety of applications.

We consider in this paper the process of orthogonal cutting that removes metal to create high quality, high precision surface shapes. This deceptively simple process actually involves complex phenomena crossing the fields of metallurgy, tribology, elasticity, plasticity, heat transfer and lubrication. We shall isolate the primary parameters and focus only on the effects of plasticity, friction and the geometric parameters.

---

* Graduate Student
† Professor

0029–5981/92/050365–25$12.50

Received 30 August 1990

Our goal is to derive a computational model that accurately predicts deformations, stresses, plastic strain distribution in the workpiece and the load on the tool under parameter variations including the cutting depth, cutting angle, degree of lubrication and material parameters of the workpiece. The model and the computer software must be efficient enough so that a computational project should consume much less effort and cost than an experimental test procedure. In fact, the software should be so efficient that a wide range of parameter variations can be examined to discover unexpected or less obvious optimal cutting conditions. The trend of the predicted results many lead to new designs of the process and tool machines. A survery of the literature reveals some limited successes and some shortcomings of the available methods that simulate this complex metal cutting process. Our approach adds new capability to this ongoing effort.

One of the numerical methods for simulating manufacturing processes is the finite element method based on the incremental plasticity theory. For metal cutting problems, an incremental analysis must be carried to the limit load condition so that the workpiece begins to flow steadily under a constant loading condition. In a cutting process, the workpiece moves at a constant speed relative to the tool and the steady state flow is maintained. To reach this condition, the incremental analysis computes a large amount of intermediate data which are of less concern to the process. Yet near the limit where the information is critical, the quality of an incremental solution deteriorates owing to numerical instability and ill-conditioning. Even although these difficulties may be remedied by *ad hoc* schemes, the intrinsic wastefulness of an incremental method remains and adds to computing cost. The questions of accuracy, uniqueness and continuity of solutions remain open in the analysis of incremental methods.

Limit analysis of plasticity[2,3] approaches the correct limit load and the associated plastic flow directly. It is derived from a certain extremum principle. Its success has already been demonstrated by the slipline method.[1,2] The only drawback lies in the graphic nature of the method and its inability to handle complex geometry and boundary conditions. We are now taking fundamental steps to remove these disadvantages.

The extremum principle, which requires the stress field to satisfy the equilibrium equation, the static boundary conditions and the material strength limit and which permits certain stress discontinuity in the deforming body, leads to the lower bound theorem.[1,2] It predicts a load either lower or equal to the exact limit load that maintains the steady motion. An approximate lower bound solution underestimates the limit load, so it is pertinent as a guide to safe designs of structures. On the other hand, the extremum principle, which requires a geometrically self-consistent flow field and permits tangential velocity discontinuity in the interior and slipping along boundaries, leads to the upper bound theorem.[1,2] An approximate upper bound solution overestimates the limit load. It may serve as a guide for designing a manufacturing machine with capacity to spare. A duality theorem equates the least upper bound to the greatest lower bound. We shall present a method that, in theory, converges iteratively to the least upper bound, the exact limit solution. In practice, we terminate computation when an iterate is deemed close enough to the limit solution.

Applications of duality theorems, the finite element method and an iterative algorithm to limit analysis have been presented for solutions of beam, frame, plate, torsion and flow problems.[3,5a-e] Analysis of the existence of a solution of the continuum problem can be found in current topics in functional analysis[3,2] and calculus of variations.[5] Convergence of an algorithm which we use for the discrete approximation of the original problem is given in Reference 3.

We now extend this methodology to the class of orthogonal metal cutting problems. Although it is a sub-class of the plane strain problems, its complicated boundary conditions and a large and distinctive set of parameters merit an independent study.

ORTHOGONAL CUTTING PROCESS

An orthogonal metal cutting process for a controlled contact tool is depicted in Figure 1 with labels illustrating the nomenclatures used in this paper. An Eulerian reference co-ordinate is used to describe the steady state motion of the workpiece relative to a stationary cutting tool. This cutting method is a common and time honoured metal removal process which produces finished surfaces with high quality. Its general use in all industries may give an impression that it is a perfected art. Yet, tool failure and product quality deterioration account for frequent and costly downtime for all cutting machines. Optimization of the process and accurate estimate of tool life become indispensible in this age of automation.

The experience based on statistical approach to improve the cutting process had been exhausted. A fundamental approach to develop a general predictive cutting theory was desired. Many simple cutting models were established in the mid 19th century. It was not until 1940 that Merchant[21] developed the earliest steady state orthogonal cutting model. He used a minimum energy hypothesis and found the relations between the shear angle and the rake angle. Applying the slipline theory, Lee and Shaffer[17] proposed another steady state orthogonal cutting model. By an assumed slipline field in the workpiece adjacent to the cutter, cutting force, chip thickness, chip deformation, shear angle and built-up edge were predicted under different friction conditions and rake angles. Shawn *et al.*[28] investigated the relations between shear angle and other operating variables. Creveling *et al.*[8] compared several published theories with experimental data and found them inconclusive with certain agreements and discrepancies.

Early studies brought certain remarkable conclusions. The shear angle was found to play an important role in the cutting process. Kececioglce[13] analysed the effects of strain rate. Kobayashi and Thomsen[16a] tested some commonly used metals and observed that the average shearing stress on the shear plane remained constant and was independent of normal stress and cutting speed (or strain rate). Eggleston *et al.*[11] investigated the shear angle relations for some materials and concluded that the relation between the shear angle and the rake angle was approximately linear. Usui and Takeyama[34] measured the stress distributions on the rake face by a photoelastic technique. They found that frictional stress was uniformly distributed over a wide range of tool–chip contact length.

Kobayashi and Thomsen[16b] reviewed various cutting theories then concluded that the actual ratio of cutting depth to chip thickness would never be greater than unity. Oxley[22] added strain-hardening to the slipline method and studied the influence of friction and rake angle on the shear zone. Meantime, Cook *et al.*[7] studied the kinematics of chip curl and the influence of built-up edge. Armarego[1] claimed that experimental shear angles were not in agreement with that

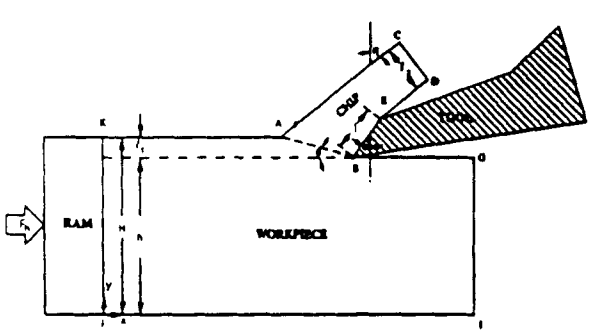

Figure 1. Schematic representation of the orthogonal cutting for a controlled contact tool

predicted by the existing theories. A modified model of Cumming *et al.*[9] improved certain correlation between analytical and experimental results. Rowe and Spick[26] proposed another model and obtained more accurate shear angles. Bailey and Boothroyd[2] reviewed some previous work and found that the mean friction stress and the mean normal stress at the tool–chip interface vary independently. Sweeney[30] offered a model to explain the relation between cutting force and shear plane. Even a brief survey of the literature will reveal the complexity of the cutting process and continuing efforts to improve inadequate aspects of the current theories.

A more extensive survey was made recently by Tyan.[33] We shall compare results with the established data but our study will focus on four control parameters, namely friction, tool geometry, rake angle and cutting depth. One parameter in the tool geometry is the tool–chip contact length. DeLeeuw[10] and Klopstock[14] first explored the advantages of controlled contact length. Takeyama and Usui[3] reported that the tool–chip contact area is a key factor and it affects cutting performance and tool life. Rake angle is another parameter which plays a significant role. Chao and Trigger[6] made extensive observations concerning the influence of these parameters in an experimental study. Kobayashi and Shabaik[15] studied the effects of cutting depth which they related to the stability of the process. We shall re-examine all their conclusions against our own. The goal is to find combinations of these parameters that achieve saving in power consumption, increase in tool life, correct lubrication method (determine tolerable friction condition) and improved surface quality (operate the process away from boundary of stability). The results presented in this paper should point out the window of optimization for this complicated metal cutting process.

We make some basic assumptions to derive a simple yet realistic model. A perfectly plastic workpiece (which may harden) in the sense of asymptotic yield behaviour is assumed. The von Mises yield criterion is used so we may compare results with others. An elastic law is not needed in the formulation, although the elastic deformation is not explicitly excluded. Continuous chip formation is assumed since the workpiece is modelled to be infinitely ductile. The effects of strain rate and temperature are not considered. The edge of the cutter is perpendicular to the direction of motion (definition of orthogonal cutting). The cutting depth is assumed small compared with the width of the cutting edge so the deformation is mainly in a plane strain mode. Since a controlled contact tool is used, a full contact of chip with the rake surface is assumed and the constant shear stress factor is adopted as a model of interface friction. The tool is assumed rigid. The tool tip has zero radius of curvature and the tool flank clearance angle is large enough such that there is no contact between the workpiece and the flank surface.

PRIMAL FORMULATION

The plane strain model shown in Figure 1 consists a workpiece of thickness H moving toward a stationary tool at a constant speed while a chip thickness t_2 is being cut away. A layer of large shear deformation occurs along the plane AB (the shear plane) inclined at an angle ϕ (shear angle) to the horizontal line. The width of the chip is assumed to be large as compared with the cutting depth t_1 and the chip thickness t_2. The plane strain condition made the model two dimensional. We use a controlled contact tool which limits the actual contact length to the artificially controlled contact length l.

Chip flow direction is represented by a variable η called chip stream angle. The chip, after passing the tool, moves as a rigid body and is no longer of concern to the present study. In the actual process, the chip stream produces a curl downstream. The chip stream angle η together with the chip thickness t_2 suffice to describe the chip geometry and to determine either forward or backward downstream curl. The shear angle ϕ is assumed to depend on the chip geometry as shown in Figure 1. For a given cutting depth t_1, chip thickness t_2, rake length l, chip stream angle

η and rake angle α, the shear angle ϕ is uniquely determined by the geometrical equation

$$\tan\phi = \frac{t_1 \cos\eta}{l\sin(\eta - \alpha) + t_2 - t_1 \sin\eta} \tag{1}$$

When the chip stream angle η is equal to the rake angle α, the above equation reduces to $\tan\phi = t_1\cos\alpha/(t_2 - t_1\sin\alpha)$, which is a special case of (1) used by many researchers. For most controlled contact tools, the chip stream angle is larger than or equal to the rake angle. In some cases, the controlled contact length may be greater than the actual contact length such that the chip curls backwards before it reaches the end of the rake surface (point E in Figure 1). The model defined in Figure 1 will be used in our mathematical formulations.

An Eulerian co-ordinate system is used for the steady state plastic flow described in the model. Under the plane strain assumption, all variables are functions of (x, y), the co-ordinates in a cross-sectional plane of the flow. The non-trivial equilibrium equations in the absence of body force can be written in matrix notation

$$\nabla\cdot\boldsymbol{\sigma}(x, y) = 0 \quad (x, y)\in D \tag{2}$$

where D is the domain of the model which is chosen to be large enough to include all plastically deforming regions in the flow, outside which the flow is in rigid body motion, where $\nabla\cdot$ is the two dimensional divergence operator and $\boldsymbol{\sigma}\in R^{2\times 2}(D)$ is the matrix function of stress distribution,

$$\boldsymbol{\sigma} = \begin{bmatrix} \sigma_{xx}(x, y) & \sigma_{xy}(x, y) \\ \sigma_{yx}(x, y) & \sigma_{yy}(x, y) \end{bmatrix} \tag{3}$$

The component σ_{zz} is also a function of (x, y) and is equal to $\frac{1}{2}(\sigma_{xx} + \sigma_{yy})$ under the plane strain condition.

The static boundary conditions consist of the prescribed traction on the workpiece exerted by the ram, the friction force exerted by the tool and the traction free boundary condition such that

$$\boldsymbol{\sigma}\cdot\mathbf{n} = \mathbf{f}\left(\frac{F_h}{H}, \tau_s\right) \quad \text{on } \partial D_s \tag{4}$$

where ∂D_s is part of the boundary of D on which the above mentioned static boundary conditions are applied; $\mathbf{n}$ is the unit outward normal vector on ∂D_s; F_h denotes the total horizontal cutting force exerted by the ram and τ_s is the frictional shear stress on the tool–strip interface. The stress free boundary condition is implied in (4). The stress distributions that satisfy (2) and (4) are called statically admissible.

We assume that the workpiece has an asymptotic yield behaviour that follows the von Mises yield criterion expressed by

$$\|\sigma\|_v \leqslant 2k \tag{5}$$

where $\|\sigma\|_v$ denotes the von Mises yield function in the form of a seminorm[35f] on the stress matrix and k is the asymptotic yield stress, a material constant. The equation (5) defines those stress states which are constitutively admissible.

In the lower bound theorem, an admissible stress state is both statically and constitutively admissible. An extremum of such states which maximizes F_h gives the exact limit load. The constrained maximization problem,

$$\begin{aligned} &\text{maximize } F_h(\sigma) \\ &\text{subject to } \nabla\cdot\boldsymbol{\sigma} = 0 \quad \text{in } D \\ &\qquad\qquad \boldsymbol{\sigma}\cdot\mathbf{n} = \mathbf{f} \quad \text{on } \partial D_s \\ &\qquad\qquad \|\sigma\|_v \leqslant 2k \quad \text{in } D \end{aligned} \tag{6}$$

is the primal (natural) formulation for the described model problem with controlled contact tool. The problem (6) is also called the lower bound formulation.

The primal formulation can be discretized first by a finite element method[36] and then solved by a method of non-linear programming.[20] The extremum of the problem is unique but the corresponding stress distribution may or may not be. There are well-known examples in limit analysis where limit solutions in terms of stress distributions and velocity fields are not unique but the limit load is always unique. We need to bring in the velocity fields through the dual formulation.

KINEMATIC BOUNDARY CONDITIONS AND DUAL FORMULATION

Using the principle of virtual work, the equilibrium equation (2) can be rewritten in a weak form

$$\int_D \mathbf{u}\cdot(\nabla\cdot\boldsymbol{\sigma})\,\mathrm{d}A = 0 \quad \forall \mathbf{u}\in K \tag{7}$$

where $\mathbf{u} = (u(x, y), v(x, y))$ is an arbitrary vector function in $R^2(D)$ which satisfies the prescribed kinematic boundary conditions on a certain boundary ∂D_k of D, K is the set of all kinematically admissible functions which satisfy the kinematic boundary conditions and the incompressibility condition implied by the constitutive model.

Integrating by parts using the divergence theorem, we may rewrite equation (7) in the form

$$\oint_{\partial D} \mathbf{n}\cdot\boldsymbol{\sigma}\cdot\mathbf{u}\,\mathrm{d}S - \int_D \boldsymbol{\sigma}:\nabla\mathbf{u}\,\mathrm{d}A = 0 \tag{8}$$

where $\mathbf{n}$ is a unit outward normal vector on the boundary of D, the symbol : denotes the inner product operator between two matrices and $\nabla\mathbf{u}$ is the velocity gradient in the form of a 2×2 matrix function defined in D.

The line integral in (8) covers the enitre boundary which shall be decomposed into six segments according to Figure 1, such that

$$\partial D = \bigcup_{i=1}^{6} \partial D_i \tag{9}$$

where ∂D_1 (line segment JK) is the ram–workpiece contact surface with velocity $(u, v) = (u_r, 0)$ (u_r being the ram velocity); ∂D_2 (segment EB) is the chip–tool contact surface with velocity boundary condition $(u_n, u_t) = (0, u_s)$ (u_s remains unknown); $\partial D_3 = \mathrm{KAC} \cup \mathrm{DE} \cup \mathrm{BG}$ is the union of all traction free boundaries; ∂D_4 (segment CD) is the chip-top surface with velocity $(u_n, u_t) = (u_c, 0)$ (u_c being the unknown chip velocity); ∂D_5 (segment GI) is the workpiece outlet boundary, which is also traction free but has a velocity $(u, v) = (u_r, 0)$ since the part of the D below the tool moves mainly as a rigid body; ∂D_6 (segment IJ) is the bottom surface of the workpiece where the velocity boundary condition fits also the rigid body motion, $(u, v) = (u_r, 0)$. If we treat some of the boundary velocities as unknowns, there is no contradiction in using them as kinematic boundary conditions.

The line integration in (8) may be carried out piecewise in each of the segments. Non-zero contributions will come only from the first two segments. They are

$$\begin{aligned} \int_{\partial D_1} \mathbf{n}\cdot\boldsymbol{\sigma}\cdot\mathbf{u}\,\mathrm{d}S &= F_h u_r \\ \int_{\partial D_2} \mathbf{n}\cdot\boldsymbol{\sigma}\cdot\mathbf{u}\,\mathrm{d}S &= -mk\int_0^t |u_s|\,\mathrm{d}s \end{aligned} \tag{10}$$

In the second integral, the constant friction model $\tau_s = mk$, $0 \leqslant m \leqslant 1$ is used where m is the friction

factor representing the lubrication condition, with $m = 0$ for perfect lubrication and $m = 1$ for sticking. The tangent velocity $u_s(s)$ of the chip along the rake surface remains unknown and becomes a part of the minimizer in the dual formulation.

The second integral in (8) can be simplified by the use of the incompressibility condition and a certain split on stress and velocity gradient matrices. The stress matrix can be split into hydrostatic and deviatoric parts and the velocity gradient matrix can be split into strain rate and spin rate such that

$$\boldsymbol{\sigma} = \sigma_m \mathbf{I} + \mathbf{S}$$

$$\nabla \mathbf{u} = \boldsymbol{\varepsilon} + \boldsymbol{\omega}$$

where σ_m is the hydrostatic stress component, $\mathbf{I}$ is the 2×2 identity matrix, $\mathbf{S}$ is the deviatoric stress matrix, $\boldsymbol{\varepsilon}$ is the strain rate matrix and $\boldsymbol{\omega}$ is the spin rate matrix.

Using the incompressibility condition, $\mathbf{I}:\boldsymbol{\varepsilon} = 0$, the property of skew symmetry of $\boldsymbol{\omega}$, $\boldsymbol{\sigma}:\boldsymbol{\omega} = 0$ and the matrix splitting above, we have the identity

$$\boldsymbol{\sigma}:\nabla \mathbf{u} = \mathbf{S}:\boldsymbol{\varepsilon} \tag{11}$$

Since the von Mises yield criterion is invariant to hydrostatic stress, $\|\sigma\|_v = \|\mathbf{S}\|_v$. The generalized Hölder inequality,[35f] when applied to (11), yields

$$|\boldsymbol{\sigma}:\nabla \mathbf{u}| = |\mathbf{S}:\boldsymbol{\varepsilon}| \leqslant \|\sigma\|_v \|\varepsilon\|_A \leqslant 2k\|\varepsilon\|_A \tag{12}$$

where $\|\varepsilon\|_A = \frac{1}{2}\sqrt{\varepsilon:\varepsilon}$ is the dual von Mises norm[35f] applied to the strain rate matrix.

Substituting (10) and (12) into (8) and rearranging terms, we obtain the following inequality:

$$F_h(\sigma) \leqslant 2k \int_D \|\varepsilon\|_A \, dA + mk \int_0^l |u_s| \, ds = \bar{F}_h(\mathbf{u}) \tag{13}$$

We have established $\bar{F}_h(\mathbf{u})$ as an upper bound functional to the original functional $F_h(\sigma)$ to be maximized in (6). Since the inequality is sharp, the least upper bound recovers the maximum of F_h. Since $\bar{F}_h$ is a function of $\mathbf{u}(x, y)$ only, we seek a kinematically admissible $\mathbf{u} \in K$ which minimizes $\bar{F}_h$ and leads to the duality theorem,

$$\min_{\mathbf{u} \in K} \bar{F}_h(\mathbf{u}) = F_h^* = \max_{\sigma \in L} F_h(\boldsymbol{\sigma})$$

where F_h^* is the limit cutting load to be delivered by the ram and L denotes the set of all functions $\sigma(x, y)$ which are statically and constitutively admissible.

Since we have used a strain rate independent yield model, the ram velocity does not affect the results of the cutting process. We may normalize the ram velocity by letting $u_r H = 1$. The dual problem may now stated in the form

$$\begin{aligned} &\text{minimize } \bar{F}_h(\mathbf{u}) \\ &\text{subject to } \bar{F}_h = 2k \int_D \|\varepsilon\|_A \, dA + mk \int_0^l |u_s| \, ds \\ &\qquad u_r H = 1 \\ &\qquad \frac{\partial u}{\partial x} + \frac{\partial v}{\partial y} = 0 \\ &\qquad \text{kinematic boundary conditions} \end{aligned} \tag{14}$$

The problem (14) can be written in terms of velocity components explicitly, and the upper bound functional, when divided by the material constant k, can be made dimensionless. This can be easily accomplished by replacing the functional in (14) with

$$\tilde{F}_h = \int_D \sqrt{\left(\frac{\partial u}{\partial x} - \frac{\partial v}{\partial y}\right)^2 + \left(\frac{\partial u}{\partial y} + \frac{\partial v}{\partial x}\right)^2}\, dA + m \int_0^l |u_s|\, ds$$

where $\tilde{F}_h = \bar{F}_h/k$ is the normalized upper bound functional.

Sometimes it is convenient to write the dual formulation in terms of a stream function instead of velocity components. The stream function $\psi(x, y)$ which satisfies the incompressibility condition automatically is defined by

$$u = \frac{\partial \psi}{\partial y} \quad \text{and} \quad v = -\frac{\partial \psi}{\partial x} \tag{15}$$

In a complete analysis of the cutting process, both the velocity and the stream function need to be computed; we choose the velocity formulation (14) and compute the stream function afterwards using (15).

FINITE ELEMENTS AND NUMERICAL ALGORITHM

A finite element method is used to approximate the dual formulation. We chose the nine-node Lagrangian isoparametric quadrilateral element to discretize the velocity function in terms of a set of interpolation functions. This element has been demonstrated to give accurate results in many finite element approaches to flow problems.[36] One of the characteristics of this element is that the sides of this element are allowed to fit curved boundaries more easily. This has an advantage in describing the chip portion of the domain. On the other hand, the velocities across elemental boundaries are assumed continuous. As a result, a solution with a discontinuous velocity field, as it may well be in cutting problems, can not be captured exactly by this element, but a high gradient at the velocity discontinuity will be obtained instead. The detailed derivation of the algebraic approximation of (14) is contained in Reference 33. We shall present the finite dimensional minimization problem, which approximates the dual formulation (14), after a slight notational fix.

To avoid proliferation of notations, we denote the upper bound functional in a finite dimensional space with the same symbol, $\tilde{F}_h$, except that it is now a function (instead of a functional) of a vector U which is the finite dimensional approximation of $\mathbf{u}(x, y)$. Using a penalty parameter β, we may bring the incompressibility condition into the upper bound function such that

$$\begin{aligned} \bar{F}_h(U) &= U^t K_1 U + mU^t K_2 U + \beta U^t K_3 U \\ &= U^t K U \end{aligned} \tag{16}$$

where K_1, K_2 and K_3 are the global stiffness matrices which arise from the contributions of plastic deformation in D, the friction boundary condition along ∂D_2 and the incompressibility condition respectively; and where $K = K_1 + mK_2 + \beta K_3$ is the combined global stiffness matrix. The matrix $K(U, m, \beta)$ also contains other geometric and material parameters implicitly. Like the stiffness matrices derived from incremental plasticity theory, K is symmetric and banded. It remains positive definite or semidefinite under limit loading conditions. This last property can not be said to hold for a stiffness matrix derived from the incremental theory.

The finite dimensional approximation of (14) is a non-linear optimization problem which is solved by a sequence of quadratic programming. K is regarded as a constant matrix at each

iterative step in the sequence. It is evaluated using the known vector U from the previous step. The initial U is, of course, a guess. The quadratic programming problem at the nth step has the form

$$\begin{aligned} &\text{minimize } \tilde{F}_h(U_n) \\ &\text{subject to } \tilde{F}_h(U_n) = U_n^t K_{n-1} U_n + U_n^t B_{n-1} \\ &\qquad u_r H = 1 \\ &\qquad n = 1, 2, \ldots \end{aligned} \tag{17}$$

in which the kinematic boundary conditions are absorbed into the constant matrix K and the constant vector B. The second constraint can be satisfied by either fixing u_r and scaling H, or by fixing H and scaling u_r. Once u_r is fixed, other components of U are scaled relative to it.

Finally, we need a stopping criterion for the sequence so it terminates in a finite number of steps with an acceptable solution. This practical convergence criterion is determined by a compromise of computing cost, accuracy requirement, ease of implementation and the law of diminishing return. We define two error measures

$$E_u = \frac{\| U_n - U_{n-1} \|_\infty}{\| U_{n-1} \|_\infty}, \quad E_f = \frac{|\tilde{F}_n - \tilde{F}_{n-1}|}{|\tilde{F}_{n-1}|}$$

and set the terminating criterion as $E_u \leqslant 10^{-5}$ and $E_f \leqslant 10^{-6}$. This criterion produced highly accurate solutions on an Apollo class microcomputer with an efficiency of one hour run time or less for each cutting condition. Generally, the time required for each case is much shorter. An approximate solution here includes the limit load, cutting force components, chip thickness, chip stream angle, chip ratio, velocity, stream function and plastic strain rate distribution. A given set of cutting conditions consists of a cutting depth, a rake length, rake angle and a friction factor. The extensive results for wide range parametric variations as well as posterior analysis and comparison will be presented in the next section.

A question should be asked in connection with any scientific software development. Does the program converge for all cases and with what initial guess? The algorithm was first developed by Liu and Yang[18] and subsequently applied to different problems in limit analysis. The algorithm converged every time with arbitrary and even deliberately constructed adverse initial iterates. This 100 per cent success rate prompted Yang and his co-worker to launch a theoretical study on convergence. They found that the blessing lies in a well known theorem in convex analysis.[25] The details of the algorithm and some recent refinements can be found in Reference 3.

RESULTS AND ANALYSIS

The material parameter k in the von Mises yield criterion appears homogeneously in the problem and is eliminated by normalizing the cutting forces with it. Eight other parameters, not all independent, define the cutting condition and response. They are: cutting depth t_1, chip thickness t_2, shear angle ϕ, friction factor m, rake angle α, rake length l, stream angle η and horizontal cutting force F_h, as shown in Figure 1. For a given cutting condition, the cutting depth t_1, rake angle α, rake length l and friction factor m are given. These are called the control parameters. The other four are part of the solution to be computed by the software. But the approximation by the finite element method requires the boundaries of the domain including the chip geometry be known *a priori*, but it is not. The remedy we provide treats the unknown parameters in chip geometry as the variables to be included in the overall solution procedure.

The boundary of the domain depends on five parameters, t_1, t_2, α, η and l. The upper bound of F_h is a function of the other seven parameters (implicit) and the velocity vector U as the relation in (17) suggests. The shear angle ϕ is given in equation (1) in terms of t_1, t_2, α, η and l. When the values of the four control parameters are given, we need only the values of t_2 and η to start the computation. They are given estimated initial values and then updated iteratively until a minimum value of $\tilde{F}_h$ is reached. The converged values of t_2, η and ϕ corresponding to the minimum $\tilde{F}_h$ finalize the chip geometry for a given cutting condition. In addition to t_2 and η, the velocity vector U is also initially assumed and updated in the iterations. We shall change the four control parameters sequentially in small steps so that the converged values to t_2, η and U in the previous case of simulation can be used as the initial estimate to start the next simulation. This method accelerates the convergence of the subsequent cases and greatly increases the efficiency of the parametric computation. The auxiliary variables like stream lines, strain rate distribution, reaction forces on the tool and the built-up edge are computed posteriorly after a converged solution is obtained.

Cutting machines with a controlled contact tool have been in use for a long time and certain practical information as rules of thumb is available. The tool–chip contact area is the source of friction drag; thus the contact length l is a major factor which affects the chip deformation and cutting forces. A cutting condition, as discussed earlier, is defined by four parameters t_1, l, α and m. Among them, α and m are independently assigned. Since t_1 and l always appear in their ratio in the model problem, the ratio, t_1/l, defined as a new parameter, facilitates some convenience. In fact, both t_1/l and its reciprocal, l/t_1, have been used in the literature.[19,27] In this study, t_1/l is chosen as a parameter. Hence, a cutting condition is controlled by three parameters t_1/l, α and m.

A grid of the finite element model is shown in Figure 2 with 170 elements and 754 nodes. A finer mesh is constructed near the tool tip where the highest strain rates are expected. The mesh becomes sparser away from the tool tip as the motion approaches that of a rigid body in the far field of the workpiece.

We shall reiterate here an implicit assumption. The controlled contact tools behave just like natural contact tools for small values of t_1/l. Therefore the choice of t_1/l should be large enough to make sure that the chip will be fully in contact with the tool. Three cutting depths, ($0{\cdot}1H$, $0{\cdot}2H$ and $0{\cdot}3H$) and four friction factors (0·0, 0·5, 0·75 and 1.0) are chosen for the parametric variation with the rake length fixed at $0{\cdot}2H$. The rake angle varies from 10° to 80° with increments of 10°. A total number of 96 cases is simulated. The results will be presented graphically and the influence of cutting depth/rake length, rake angle and friction on cutting forces, chip geometry, velocity field and reaction forces on the tool will be discussed.

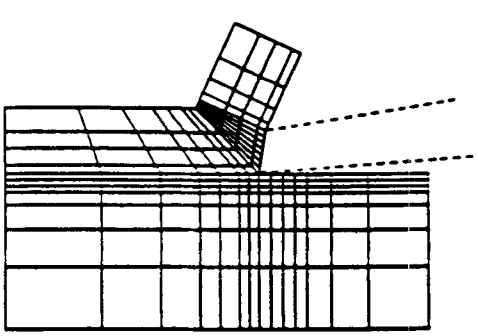

Figure 2. Finite element mesh (170 elements and 754 nodes) for $\alpha = 10°$, $t_1 = 0{\cdot}3$ and $m = 0{\cdot}5$

The cutting forces can be resolved into different orthogonal components. The resultant **R** acting on the workpiece and **R**′ on the tool are equal in magnitude but opposite in direction, so that **R** = − **R**′. They can be obtained by taking either the workpiece or the tool as a free body. The resultant force can be decomposed into normal and tangential components, N and T, with respect to the cutting surface as illustrated in Figure 3. It can also be resolved into horizontal and vertical components, F_h, F_v respectively. These components satisfy the following relations:

$$\begin{aligned} T\sin\alpha + N\cos\alpha &= F_h \\ T\cos\alpha - N\sin\alpha &= F_v \end{aligned} \tag{18}$$

F_h (its least upper bound) and T are obtained directly from simulation. Thus F_v and N can be calculated from (18) to give

$$\begin{aligned} N &= \frac{1}{\cos\alpha}(F_h - T\sin\alpha) \\ F_v &= \frac{1}{\cos\alpha}(T - F_h\sin\alpha) \end{aligned} \tag{19}$$

Furthermore, **R** can also be decomposed into components F_s and F_n respectively tangent and

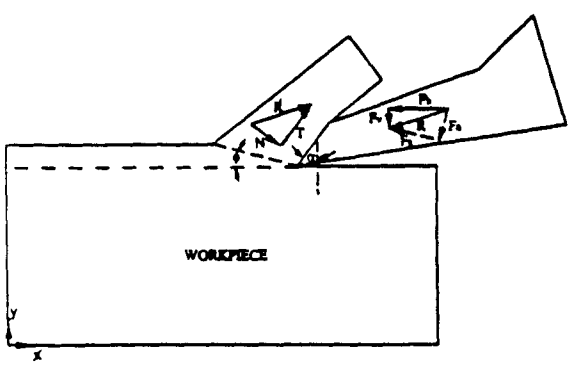

Figure 3. Resolution of resultant forces in orthogonal cutting

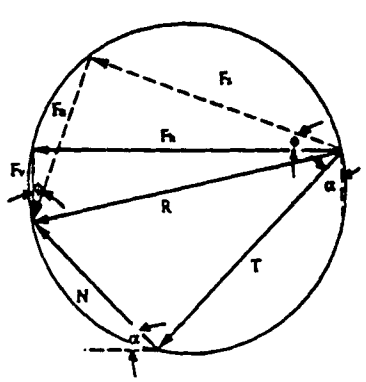

Figure 4. Composite cutting force circle

normal to the shear plane (see dashed lines in Figure 4). All the above force components can be put together to form a diagram in a single circle, called the composite cutting force circle, first suggested by Merchant.[21a] From Figure 4, it is evident that

$$F_s = F_h \cos\phi - F_v \sin\phi = F_h \frac{\cos(\alpha + \phi)}{\cos\alpha} - T\frac{\sin\phi}{\cos\alpha}$$
$$F_n = F_v \cos\phi - F_h \sin\phi = T\frac{\cos\phi}{\cos\alpha} - F_h \frac{\sin(\alpha - \phi)}{\cos\alpha} \tag{20}$$

The various components of the resultant force **R** given above will be shown in the composite cutting force circle, which is a convenient vehicle to discuss the physical phenomena implied by the numerical results.

The influence of t_1/l on cutting force components varies with friction conditions. In Figure 5, the force components F_h, F_v, T and N are plotted against t_1/l for different friction factors. For convenience of discussion, the friction factors in the range $0 < m < 1$ define intermediate friction conditions. The friction conditions corresponding to $m = 0$ and $m = 1$ are called frictionless and sticking conditions respectively.

For the frictionless condition, it is shown in Figures 5(a) and 5(b) that F_h, F_v and N are proportional to t_1/l. F_h is positive and F_v is negative for all cases. Two composite cutting circles of the same rake angle but different t_1/l ratios are sown together in Figure 6(a). It is evident that zero friction force T requires the coincidence of N and **R**. It also follows that **R** will always be perpendicular to the rake surface. The magnitude of N is proportional to t_1/l as a computed result. By rotating the α angle in Figure 6(a), the cutting force components for different rake angles are obtained. It shows that both F_h and F_v are proportional to N, so they are proportional to t_1/l as well. From the same figure, one realizes that F_h is always positive and F_v is always negative for all rake angles between 0° and 90°.

The cutting force components for the intermediate friction range are shown in Figures 5(c)–(f) which are similar to Rao, Cumming and Thomsen's theoretical predictions and experimental observations.[24] The magnitudes of F_h and N increase and F_v decreases almost linearly as t_1/l increases for the intermediate friction range. This is similar to the frictionless case except that T is now a constant. Since T is not zero, the proportionality no longer exists but the linearity is mostly preserved.

Different from the frictionless case, however, F_v is not always negative for the intermediate friction range. At small values of t_1/l and small rake angle, F_v turns positive while F_h remains positive for all cases. This change of sign of F_v can be understood from the composite cutting force circles in which two cutting conditions of $t_1/l = 0{\cdot}5$ and $t_1/l = 1{\cdot}5$ at $\alpha = 30°$ are plotted in Figure 6(b). The force components of each case are represented by a small circle with solid lines and a large circle with dotted lines respectively. For both cutting conditions the tangential force components T and T' have the same magnitude and direction since the rake length and friction condition are unchanged. Increase of t_1/l causes only increase of the normal component from N to N′. Increase of N changes the direction of the resultant **R** from downward to upward. Therefore F_v, which is the vertical component of **R**, changes its sign from positive to negative. Figure 6(b) also indicates the trend caused by friction and depth of cut. For high friction and small depth of cut, the resultant force is downward because it must overcome the upward friction force. For low friction and large depth of cut the resultant force is upward because it must tear and lift the cut material off the workpiece.

The non-linear relations between the force components and t_1/l become more pronounced under the sticking condition as shown in Figures 5(g), (h). The rates of increase of F_h, F_v and N

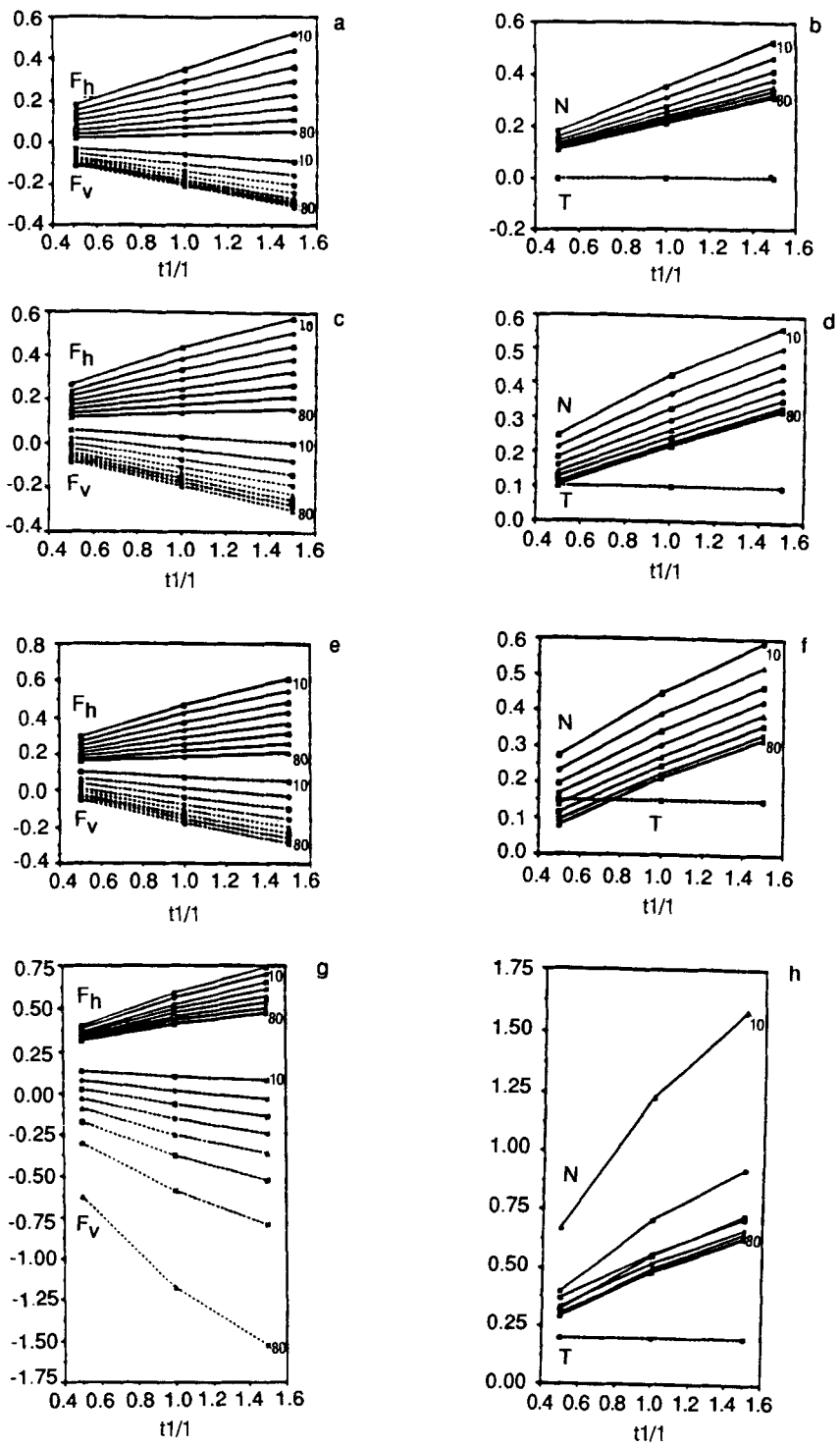

Figure 5. Predicted cutting force components versus t_1/l: (a, b) $m = 0{\cdot}0$; (c, d) $m = 0{\cdot}5$; (e, f) $m = 0{\cdot}75$; (g, h) $m = 1{\cdot}0$

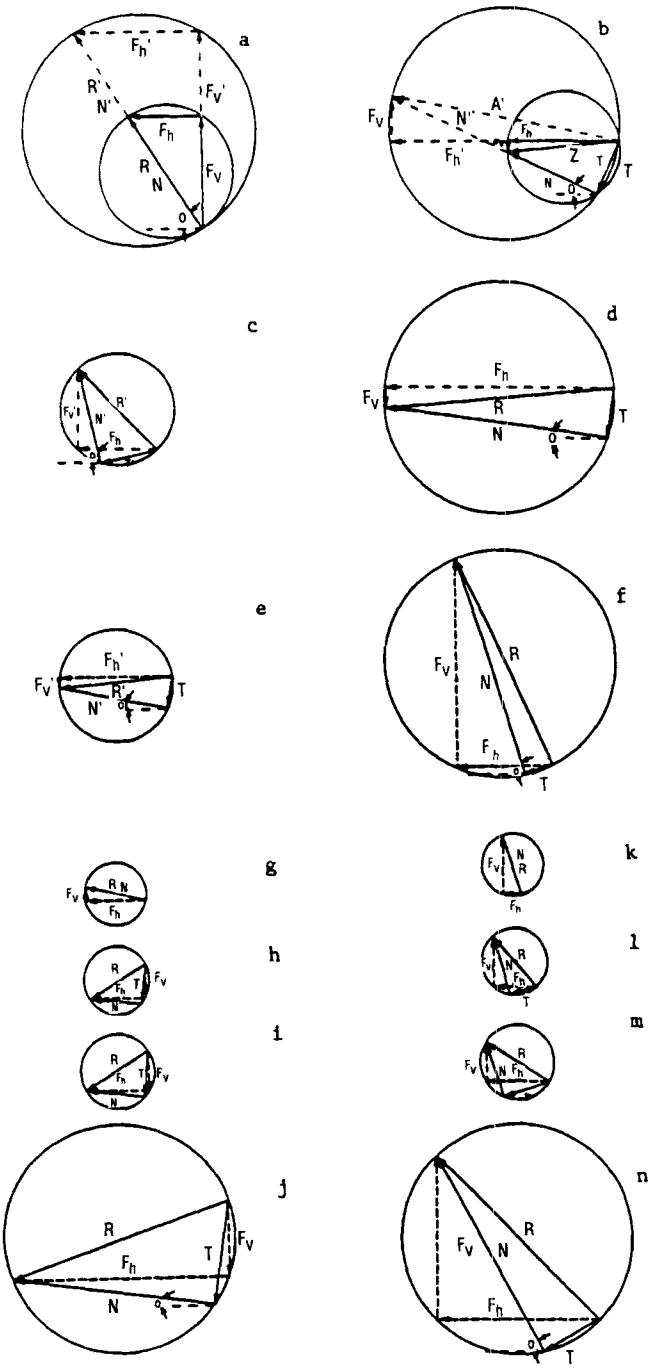

Figure 6. Composite cutting force circle for different cutting conditions

with respect to t_1/l are much higher than that for other friction conditions but the increasing rates slow down a bit at higher t_1/l. The higher increasing rates are the result of the relatively larger amount of energy dissipated in friction than in plastic deformation. The plastic deformation in a chip is homogeneous under frictionless conditions and is linearly proportional to t_1/l. The plastic deformation in the chip under large friction becomes quite inhomogeneous, thus resulting in non-linear relations for the cutting force components.

Now we shall examine the influence of rake angle on the cutting force components. The force components F_h, F_v, T and N are plotted against rake angle in Figure 7 for four friction factors. Under non-sticking conditions $m = 0{\cdot}0$, $0{\cdot}5$ and $0{\cdot}75$, both F_h and N decrease from large positive values to small positive values and F_v decreases from a small value (positive or negative) to large negative values as the rake angle increases. At small rake angles, the tool behaves more like a bulldozer blade pushing the material, so F_h and N are large and F_v is small and downward. At large rake angles, it behaves like a chisel blade tearing and lifting the material, so F_h and N are small but F_v is large and upward. To minimize the cutting forces, 90° is the optimal rake angle for all non-sticking conditions. This theoretical result is of course impractical since it requires a tool of infinitesimal thickness and thus infinite strength. A practical compromise balances tool strength and cutting forces.

For intermediate friction, F_v is positive at small rake angles and negative at large rake angles. The direction of F_v changes from downward to upward at a certain angle. We shall use two composite cutting force circles for $t_1/l = 1{\cdot}5$, $m = 0{\cdot}75$ at $\alpha = 80°$ and 10° as shown in Figure 6(c), (d) to explain this phenomenon. The component F_v is obtained by subtracting the vertical component of T from the vertical component of N is equation (18). Comparing the two circles, we realize that the vertical component of N is smaller than that of T at small rake angles while N is much larger than T. This condition is reversed at large rake angles. Therefore F_v tends to be positive at small rake angles and negative at large rake angles. The critical rake angle, at which F_v changes its direction, is a function of m and t_1/l. At this critical rake angle the mode of cutting changes from pushing to tearing.

Under the sticking condition, both F_h and F_v change monotonically, but N first decreases then increases dramatically. A minimum value of N exists between 40° and 45°. Also different from other friction conditions, the magnitudes of F_v and N are very large at large rake angles. Figures 6(e) and (f) show two composite cutting force circles for the cutting conditions of $t_1/l = 1{\cdot}5$ at $\alpha = 10°$ and 80° respectively. For the sticking condition, a larger F_h compared to other friction conditions is expected. On the rake surface (with fixed l and m), the friction force is fixed. As a result, the extra horizontal force F_h can be balanced only with increased N. At small rake angles, the direction normal to the rake surface almost coincides with the horizontal direction. Consequently, a small N is enough to balance the extra F_h. At large rake angles, the direction normal to the rake surface is almost vertical, therefore a larger N is needed to balance the extra F_h. From the non-linear trigonometric relation, a large rake angle requires a higher N to provide sufficient horizontal force component. Thus, very large values of N are found at large rake angles. F_v is the sum of vertical components of T and N. As N increases, F_v will increase accordingly. The dramatic increase of N usually causes the breaking of tools. The rake angle corresponding to minimum N value shown in Figure 7(h) provides an optimal cutting condition from the tool strength requirement viewpoint.

The influence of friction on cutting force components can be observed in Figure 8. Since a constant shear friction model is assumed, T will always be proportional to m. Other force components F_h, F_v and N are functions of m as well. As m increases, F_h increases monotonically. But F_v and N increase monotonically only for small rake angle. At large rake angles, F_v increases and then decreases while N decreases and then increases,

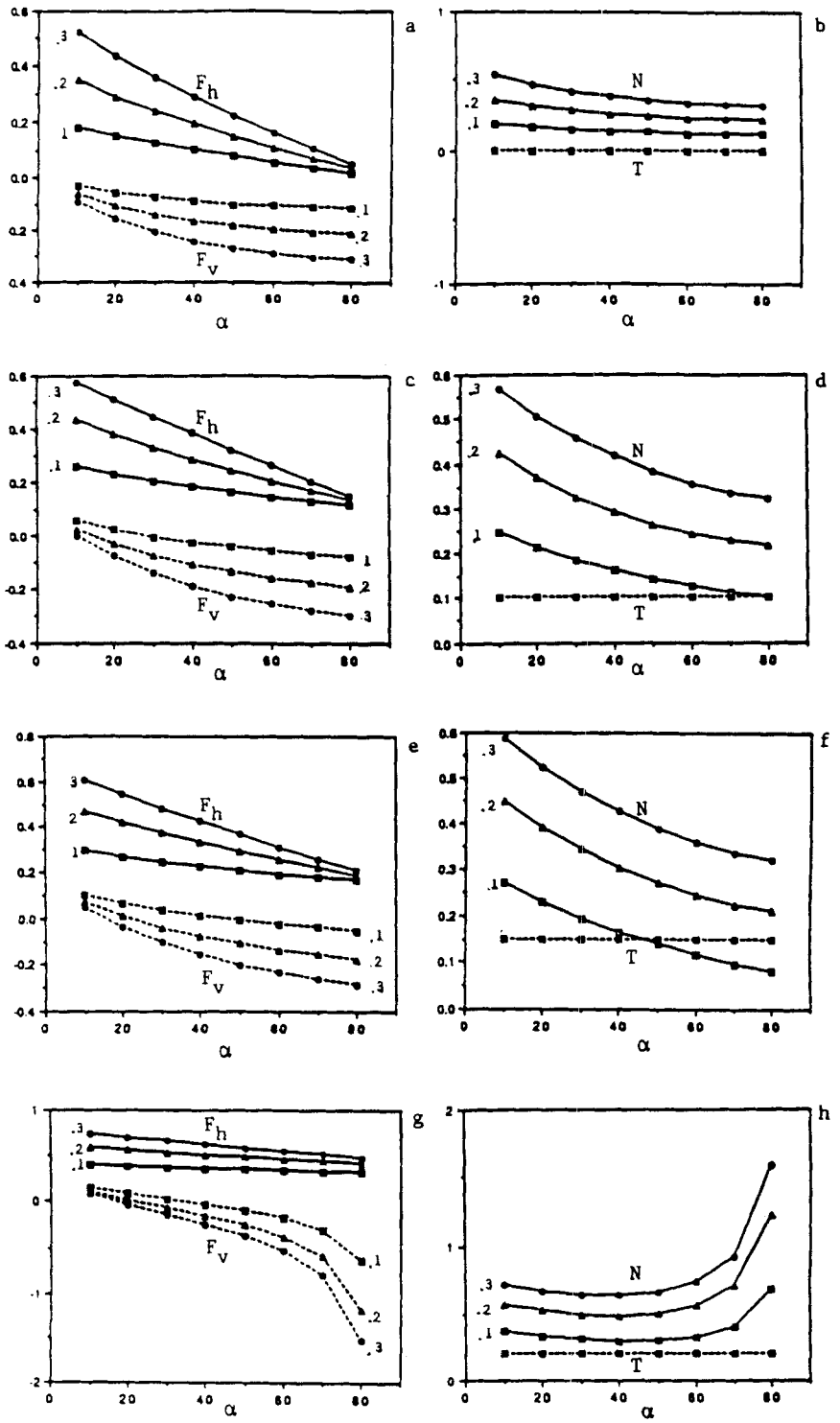

Figure 7. Predicted cutting force components versus α: (a, b) $m = 0{\cdot}0$; (c, d) $m = 0{\cdot}5$; (e, f) $m = 0{\cdot}75$; (g, h) $m = 1{\cdot}0$

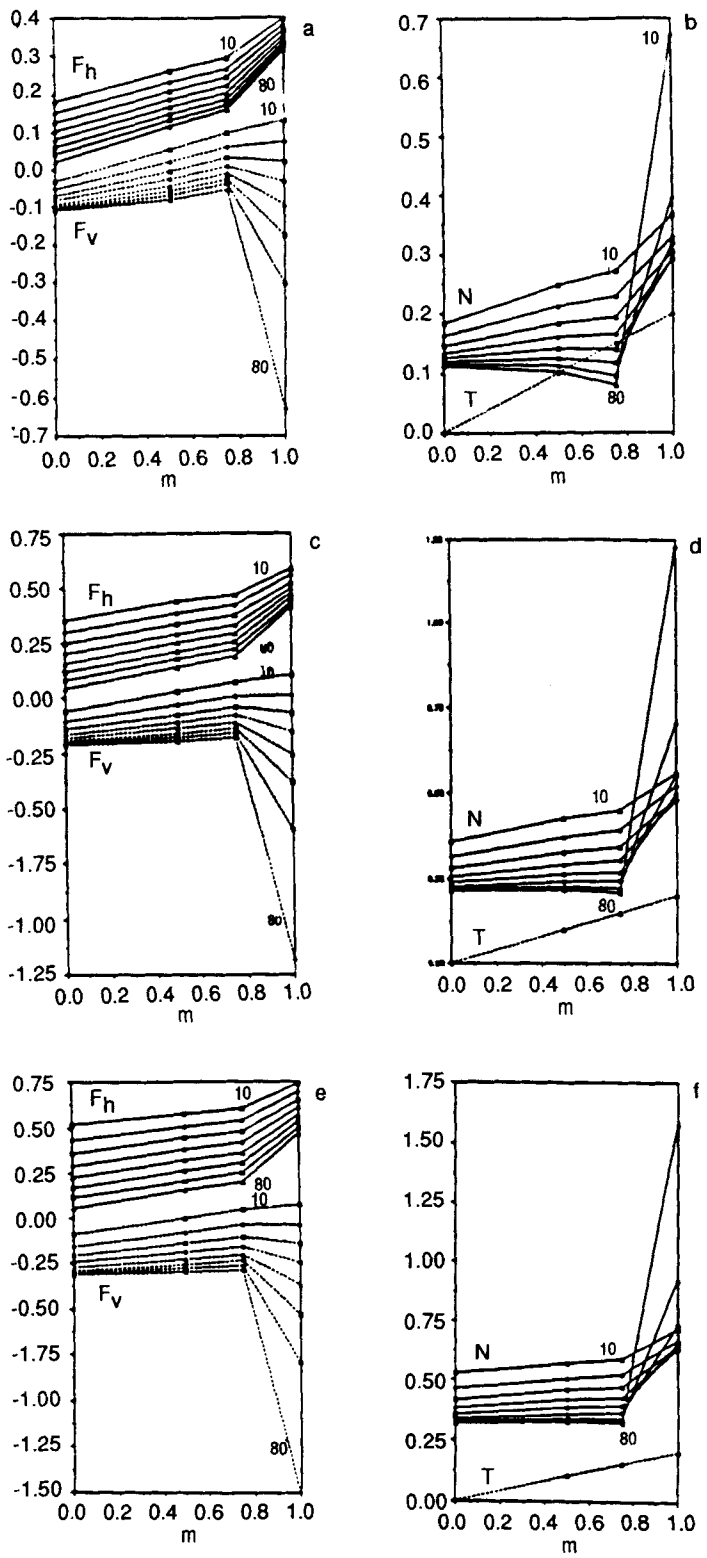

Figure 8. Predicted cutting force components versus m: (a, b) $t_1/l = 0{\cdot}5$; (c, d) $t_1/l = 1{\cdot}0$; (e, f) $t_1/l = 1{\cdot}5$

Figures 6(g)–(n), illustrate this trend. For fixed rake angle and t_1/l, larger F_h is needed to overcome higher friction. So F_h increases with m, as indicated by the numerical results. In Figures 6(g)–(n), we observe that the angle between F_v and T (also the angle between F_h and N) is equal to the rake angle. For small rake angles (Figures 6(g)–(j)), the increase of F_h and T has to be compensated by the increase of both F_v and N. So, the value of F_v increases from negative to positive and N increases from small value to large value, as m increases. The angles between F_v and T and between F_h and N are large for large rake angles (Figures 6(k)–(m)). But the angles between F_v and N and between F_h and T are small. However F_v and N are perpendicular to F_h and T respectively. Thus the increase of F_h is compensated by the increase of T. Because the increasing rate of T with respect to m is greater than that of F_h under non-sticking conditions, the magnitudes of F_v and N decrease as m increases. Since F_v is negative and N is positive, the value of F_v increases and the value of N decreases.

For frictions close to sticking condition and at large rake angle, the increasing rate of T with respect to m is smaller than that of F_h, as shown in Figure 6(n). Since F_v and N are perpendicular to F_h and T respectively, very large magnitudes of F_v and N are needed to compensate the high increasing rate of F_h. Consequently, F_v decreases and N increases dramatically at sticking conditions and large rake angles as shown in Figures 7(e), (f).

The influence of the ratio t_1/l on chip stream angle and chip thickness also varies with different friction conditions. The chip stream angle and chip thickness are plotted against t_1/l for different friction conditions in Figure 9. Under frictionless conditions (Figures 9(a), (b)), the value of t_1/l does not affect the chip stream angle and chip thickness. The chip stream angle is the same as the rake angle and the chip thickness is the same as the cutting depth for all such cases. The undeformed material transforms into the deformed chip after passing the primary shear zone. Thereafter, the deformed chip flows as a rigid body. Only in the frictional cases, is the chip thickness further increased by the friction force imparted on the chip by the tool along the rake surface. Then the large shear deformation in the chip and the friction force cause the chip to bend toward the tool. The large shear deformation also produces a chip thickness which is greater than the cutting depth, as mentioned earlier, and was reported by Kobayashi and Thomsen.[16b]

For a low friction factor ($m = 0{\cdot}5$), the chip stream angle is greater than the rake angle when t_1/l is large and the rake angle is small, as shown in Figure 9(c). The chip thickness is greater than the cutting depth for all cases. A larger t_1/l value corresponds to a larger chip ratio (cutting depth/chip thickness). The results shown in Figure 9(d) agree closely with that observed by Lo *et al.*[19] Increased friction ($m = 0{\cdot}75$ and $m = 1{\cdot}0$) produces more severe shear deformation. The results in Figures 9(e)–(h) show that the chip bends more toward the tool and this phenomenon occurs in a wider t_1/l range. The chip thickness also increases more than that under low friction conditions.

For the sticking case shown in Figure 9(g), the chip bends away from the tool, which indicates a feature of backward chip curl. In such a case, the control contact length is greater than the natural contact length. No numerical method simulating natural contact length has, as yet, been presented in the literature. A prediction of the condition leading to backward curl can be made from the current analysis. For a complete analysis of backward curl, a modification of the boundary condition along the rake surface allowing the separation is still needed.

The influence of the rake angle on the chip stream angle and the chip thickness are shown in Figure 10 for different friction factors m. Similar to t_1/l, the rake angle does not affect the chip stream angle and chip thickness under frictionless conditions (Figures 10(a), (b)). The reason has already been given. For low frictions, the chip bends toward the tool when the rake angle is small, as shown in Figure 10(c). The chip thickness is always greater than the cutting depth for all rake angles as shown in Figure 10(d). The chip thickness increases as the rake angle decreases. This

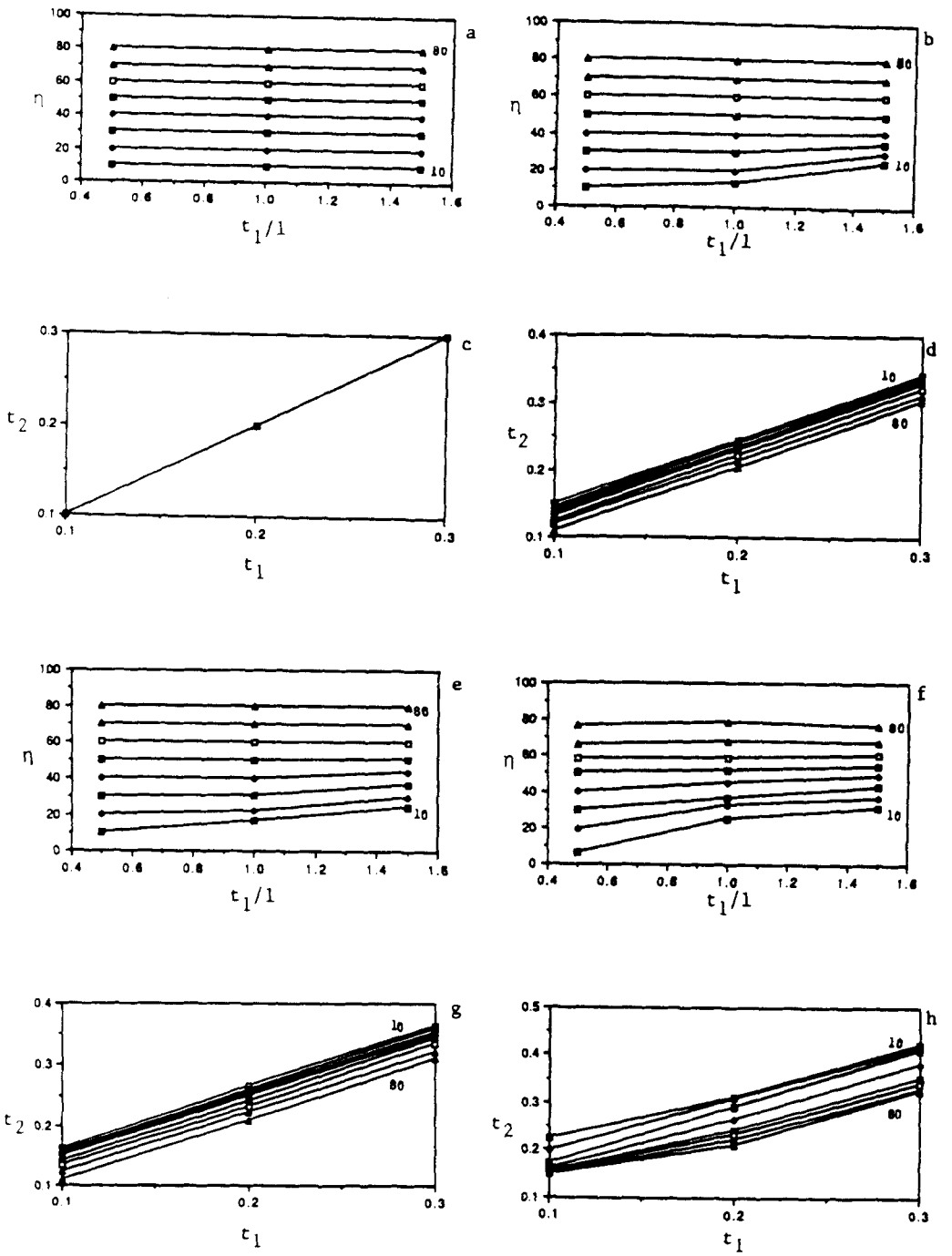

Figure 9. Predicted chip configurations versus t_1/l or t_1: (a, c) $m = 0{\cdot}0$; (b, d) $m = 0{\cdot}5$; (e, g) $m = 0{\cdot}75$; (f, h) $m = 1{\cdot}0$

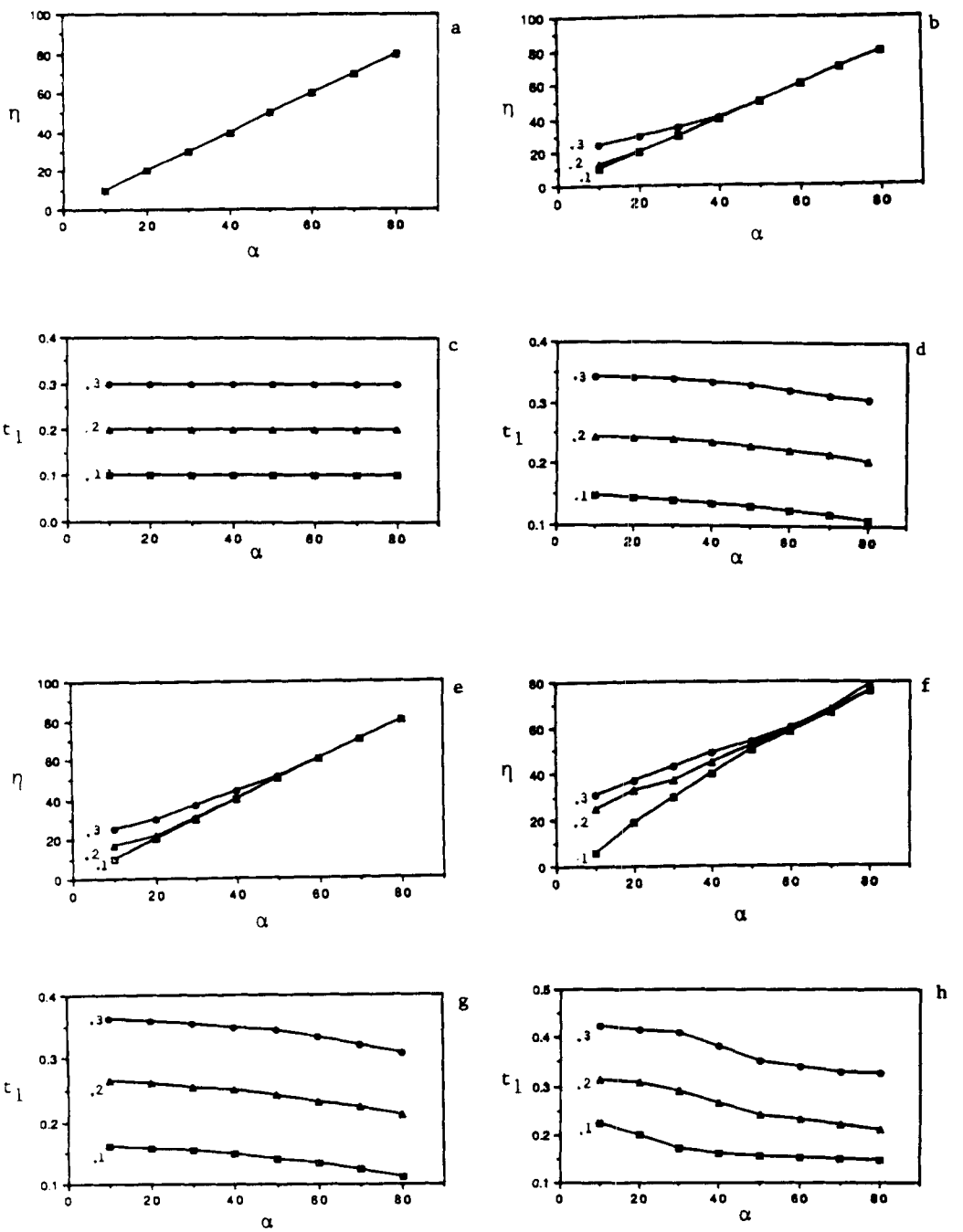

Figure 10. Predicted chip configurations versus α: (a, c) $m = 0{\cdot}0$; (b, d) $m = 0{\cdot}5$; (e, g) $m = 0{\cdot}75$; (f, h) $m = 1{\cdot}0$

agrees with the experiments of Carroll III and Strenkowski,[4] as it is obvious now that the pushing mode appears at small rake angle and the tearing mode appears at large rake angle. As the friction increases (see Figures 10(a)–(h)), this phenomenon becomes more pronounced and occurs in a wider rake angle range.

The trend of friction effect on chip stream angle and chip thickness can be observed from Figure 11. These figures illustrate the changes of chip thickness and chip stream angle due to different frictions. Greater chip thickness and larger chip stream angle are produced under higher friction for the same cutting depth and rake angle. Since higher friction causes more plastic deformation, the chip distorts more severely.

Velocity fields and the corresponding stream line diagrams for typical cutting conditions are shown in Figures 12 and 13. They are computed from the finite element mesh shown in Figure 2. The contours of effective plastic strain rate normalized with respect to its maximum value are shown in Figure 14. From these plots, the primary shear zones (shear plane) are visible at the

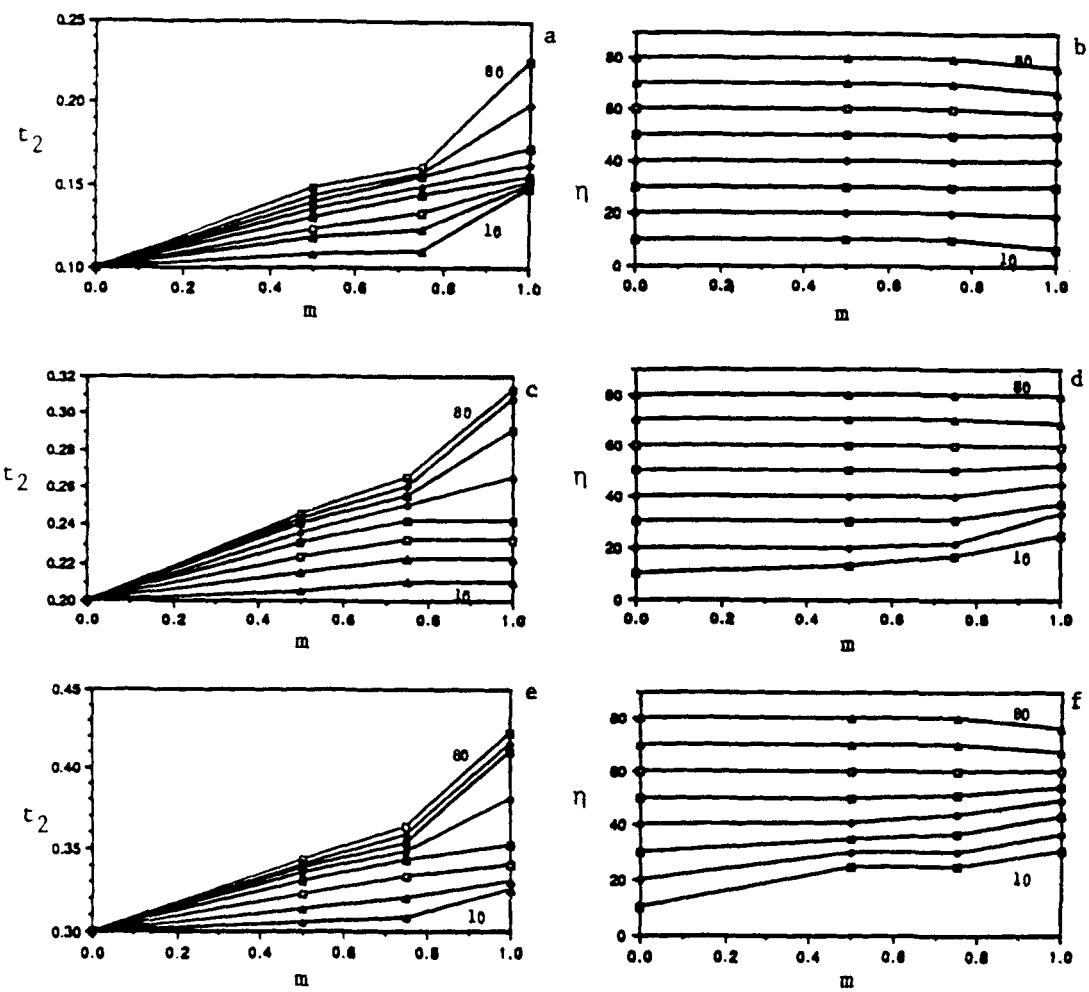

Figure 11. Predicted chip configurations versus m: (a, b) $t_1/l = 0{\cdot}5$; (c, d) $t_1/l = 1{\cdot}0$; (e, f) $t_1/l = 1{\cdot}5$

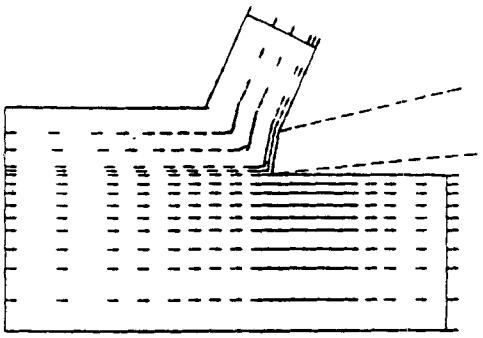

Figure 12. Velocity field for $\alpha = 10°$, $t_1 = 0{\cdot}3$ and $m = 0{\cdot}5$

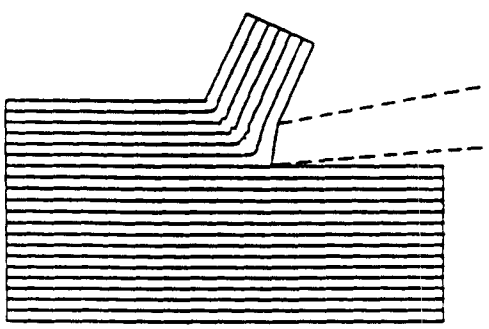

Figure 13. Streamline diagram for $\alpha = 10°$, $t_1 = 0{\cdot}3$ and $m = 0{\cdot}5$

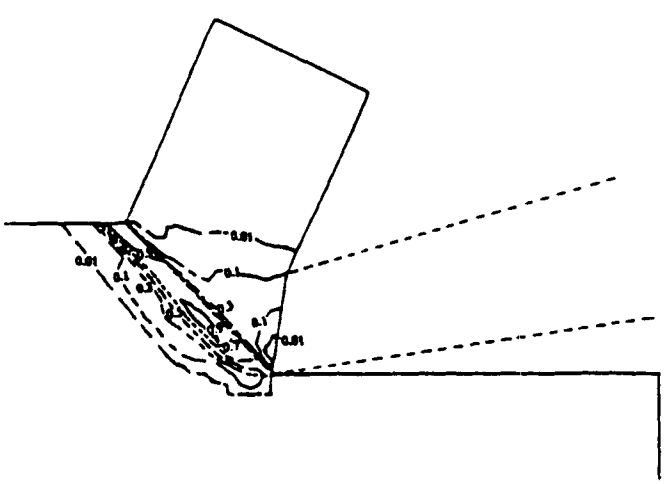

14. Effective strain rate contours for $\alpha = 10°$, $t_1 = 0{\cdot}3$ and $m = 0{\cdot}5$

bases of the chips for all cutting conditions while the secondary shear zones appear along the chip–tool interface for small rake angles and intermediate frictions as well as sticking conditions. The maximum effective plastic strain rate decreases as the rake angle increases. The predicted effective plastic strain rates are similar to that presented by Stevenson and Oxley[29] and Carroll III and Strenkowski.[4] The contours (Figure 14) also show the onset of a built-up edge (a stagnation region in the workpiece). For intermediate friction and the sticking conditions, a small region of low effective strain rate appears just above the cutting edge. This region seems to be a possible location for the formation of a built-up edge and it tends to occur at the cutting conditions of small rake angle, high friction and large cutting depth.

SUMMARY AND CONCLUSIONS

A software based on limit analysis has been developed and applied to a general class of orthogonal metal cutting problems. The minimization algorithm efficiently produced detailed results in terms of the cutting forces, chip geometry, velocity field, strain rate distribution, stream lines and the built-up edge for a wide range of cutting conditions. After comparing these results with published data obtained by other methods in limited ranges of parameters, good agreement has been confirmed. In a much wider range of parameters computed, the new results also point to the trends of the cutting process.

The relations between the variables and the four control parameters are illustrated in the figures presented. The composite cutting force circle alone provides an understanding at a glance of the changes of cutting force components under different cutting conditions. Based on the new results and analysis, we infer the following relations.

- Relation between cutting force components and t_1/l:
  1. Under frictionless conditions, the relations between F_h, F_v, N and t_1/l are linear.
  2. For intermediate friction conditions, relations between F_h, F_v, N and t_1/l are nearly linear.
  3. Under sticking conditions the rates of increase of F_h, F_v, N with respect to t_1/l are higher than those under all other friction conditions but the increasing rates slow down at higher values of t_1/l.
- Relation between cutting force components and rake angle:
  1. For all friction except sticking conditions, the values of F_h, F_v, N decrease and the slopes increase monotonically as the rake angle increases.
  2. Under sticking conditions, F_h, F_v still decrease monotonically as the rake angle increases, but N decreases first then increases abruptly as the rake angle increases. The slopes of the F_h–α and N–α curves both increase, while the slope of the F_v–α curve decreases as the rake angle increases.
  3. An optimal rake angle producing the smallest F_n is found in the range from 40° to 45° for all cutting depths under the sticking conditions.
- Relations of chip stream angle, chip thickness and t_1/l:
  1. Under frictionless conditions, the chip stream angle is the same as the rake angle and the chip thicknes is the same as the cutting thickness.
  2. For frictional cases, the chip bends toward the tool after passing the chip–tool interface at high t_1/l and small rake angle, while the chip thickness is greater than the cutting depth.
  3. As the friction increases, this forward chip bending phenomenon becomes more pronounced and occurs in a wider range of the parameters.

For a better understanding of the metal cutting process, visualization of velocity field, strain rate contours, stream lines and built-up edge is most helpful. To limit the length of the paper, only one set of velocity field, the stream lines and the strain rate distribution is presented for a typical cutting condition. The strain rate contours show a dominant zone and a secondary shear zone of plastic deformation. A primary shear zone appears in all cutting conditions. A secondary shear zone appears for small rake angles and greater friction factors including sticking. A built-up edge tends to be established at the cutting conditions of small rake angle, high friction and large cutting depth.

The computational results presented in this paper are only a few samples of what the software can deliver. The large number of parameters made it impossible to cover all cases in a technical paper, although we have computed the extreme and middle cases. The graphs use linear interpolation for all other cases. For accurate simulation of a specific cutting condition, the software will be made available to researchers whose goal is to optimize a particular cutting process. The new software presents a tool for simulating and analysing the cutting process and for optimizing the cutting conditions and tool-machine designs.

REFERENCES

1. E. J. A. Armarego, 'A note on the shear relation in orthogonal cutting', *Int. J. Machine Tool Des. Res.*, **6,** 139–141 (1966).
2. J. A. Bailey and G. Boothroyd, 'Critical review of some previous work on the mechanics of the metal cutting process', *J. Eng. Indust.*, **90,** 54–62 (1968).
3. A. Bental, M. Teboulle and W. H. Yang, 'A combined smoothing successive approximation for limit analysis problems', *Math. Programming*, to appear.
4. J. T. Carroll III and J. S. Strenkowski, 'Finite element models of orthogonal cutting with application to single point diamond turing', *Int. J. Mech. Sci.*, **30,** 899–920 (1988).
5. L. Cesari, P. Brandi and A. Salvadori, 'Existence theorems for multiple integrals of the calculus of variations for discontinuous solutions', *Annali. Mat. Pura Appl.*, (4) **152**, 95–121 (1988).
6. B. T. Chao and K. J. Trigger, 'Controlled contact cutting tools', *J. Eng. Indust.*, **81,** 139–151 (1959).
7. N. H. Cook, P. Jhaveri and N. Nayak, 'The mechanism of chip curl and its importance in metal cutting', *J. Eng. Indust.*, **85,** 374–380 (1963).
8. J. H. Creveling, T. F. Jordan and E. G. Thomsen, 'Some studies of angle relationships in metal cutting', *Trans. ASME*, **79,** 127–138 (1957).
9. J. D. Cumming, S. Kobayashi and E. G. Thomsen, 'A new analysis of the forces in orthogonal metal cutting', *J. Eng. Indust.*, **87,** 480–486 (1965).
10. A. L. DeLeeuw, *Metal Cutting Tools*, McGraw-Hill, New York, 1922, p. 18.
11. D. M. Eggleston, R. P. Herzog and E. G. Thomsen, 'Observations on the angle relationships in metal cutting', *J. Eng. Indust.*, **81,** 263–279 (1959).
12. R. Hill, *The Mathematical Theory of Plasticity*, Oxford University Press, Oxford, 1950.
13. D. Kececioglce, 'Shear strain rate in metal cutting and its effects on shear flow stress', *Trans. ASME*, **80,** 158–168 (1958).
14. H. Klopstock, 'Recent investigations in turning and planing and a new form of cutting tool', Paper presented at *ASME Spring Meeting*, 1925.
15. S. Kobayashi and A. Shabaik, 'Chip formation with varying undeformed chip thickness at very low speed', *J. Eng. Indust*, **84,** 389–394 (1964).
16. S. Kobayashi and E. G. Thomsen, (a) 'Some observations on the shearing process in metal cutting', *J. Eng. Indust.*, **81,** 251–262 (1959); (b) 'Metal cutting analysis part I: re-evaluation and new method of presentation of theories, part II: New parameters', *ibid.*, **84,** 63–70, 71–80 (1962).
17. E. H. Lee and B. W. Shaffer, 'The theory of plasticity applied to problem of machining', *J. Appl. Mech.*, **18,** 405–413 (1951).
18. K. H. Liu and W. H. Yang, 'A finite element method for limit analysis of plane strain extrusion through square dies', *Num. Meth. Indus. For. Proc.*, 1989, pp. 191–196.
19. S. Y. Lo, U. Lode and E. J. A. Armarego, 'Experiments with controlled contact tools', *Int. J. Machine Tool Des. Res.*, **6,** 115–127 (1966).
20. D. G. Luenberger, *Introduction to Linear and Nonlinear Programming*, Addison-Wesley, Reading, MA, 1973.
21. M. E. Merchant, (a) 'Mechanics of metal cutting process: Part I orthogonal cutting and a type-2 of chip', *J. Appl. Phys.*, **16,** 267–275 (1945); (b) 'Part II plasticity consideration on orthogonal cutting', *ibid.*, **16,** 318–324 (1945).
22. P. L. B. Oxley, 'Mechanics of metal cutting for a material of variable flow stress', *J. Eng. Indust.*, **85,** 339–345 (1963).

23. W. Prager, *An Introduction to Plasticity*, Addison-Wesley, Reading, MA, 1959.
24. U. M. Rao, J. D. Cumming and E. G. Thomsen, 'Some observation on the mechanics of orthogonal cutting of Delrin and Zytel plastic', *J. Eng. Indust.*, **86,** 117–121 (1964).
25. R. T. Rockafellar, *Convex Analysis*, Princeton University Press, 1970.
26. G. W. Rowe and P. T. Spick, 'A new approach to determination of the shear plane angle in machining', *J. Eng. Indust.*, **89,** 530–538 (1967).
27. C. Rubenstein, 'The mechanism of orthogonal cutting with controlled contact tools', *Int. J. Machine Tool Des. Res.*, **8,** 203–216 (1968).
28. M. C. Shawn, N. H. Cook and I. Finnie, 'The shear angle relationship in metal cutting', *Trans. ASME*, **75,** 273–288 (1953).
29. M. G. Stevenson and P. L. B. Oxley, 'An experimental investigation of the influence of speed and scale on the strain rate in a zone of intense plastic deformation', *Proc. Inst. Mech. Eng.*, **184,** 561–576 (1969–70).
30. G. Sweeney, 'The consistency of experimental observations with a model for the metal cutting process', *Int. J. Machine Tool Des. Res.*, **9,** 309–319 (1969).
31. H. Takeyama, and E. Usui, 'The effect of tool chip contact area in metal machining', *J. Eng. Indust.*, **80,** 1089–1096 (1958).
32. R. Temam, *Mathematical Problems in Plasticity*, Gauthier-Villars, Paris, 1985.
33. T. Tyan, 'Simulation and optimization for metal forming processes: cutting, rolling and extrusion', *Ph.D. Thesis*, University of Michigan, 1990.
34. E. Usui and H. Takeyama, 'Photoelastic analysis of machining stress', *J. Eng. Indust.*, **82,** 303–308 (1960).
35. W. H. Yang, (a) 'On a class of optimization problems for framed structures', *Comp. Methods Appl. Mech. Eng.*, **15,** 85–98 (1978); (b) 'A variational principle and an algorithm for limit analysis of beams and plates', *ibid.*, **33,** 575–582 (1982); (c) 'A duality theorem for plastic plates', *Acta Mech.*, **69,** 177–193 (1987); (d) 'Pipe flow of plastic materials', *J. Appl. Mech.*, **47,** 496–498 (1980); (e) 'A duality theorem for plastic torsion', *Int. J. Solids Struct.*, to appear; (f) 'The generalized Hölder inequality', *J. Nonlinear Anal.*, to appear.
36. O. C. Zienkiewicz, *The Finite Element Method*, 3rd edn, McGraw-Hill, London, 1977.